Control-Theoretic Cyber-Physical System Modeling and Synthesis: A Case Study of an Active Direct Methanol Fuel Cell

DONGHWA SHIN, JAEHYUN PARK, YOUNGHYUN KIM, JAEAM SEO, and NAEHYUCK CHANG, Seoul National University, Korea

A joint optimization of the physical system and the cyber world is one of the key problems in the design of a cyber-physical system (CPS). The major mechanical forces and/or chemical reactions in a plant are commonly modified by actuators in the balance-of-plant (BOP) system. More powerful actuators requires more power, but generally increase the response of the physical system powered by the electrical energy generated by the physical system. To maximize the overall output of a power generating plant therefore requires joint optimization of the physical system and the cyber world, and this is a key factor in the design of a CPS.

We introduce a systematic approach to the modeling and synthesis of a CPS that emphasize joint power optimization, using an active direct methanol fuel cell (DMFC) as a case study. Active DMFC systems are superior to passive DMFCs in terms of fuel efficiency thanks to their BOP system, which includes pumps, air blowers, and fans. However, designing a small-scale active DMFC with the best overall system efficiency requires the BOP system to be jointly optimized with the DMFC stack operation, because the BOP components are powered by the stack. Our approach to this synthesis problem involves i) BOP system characterization, ii) integrated DMFC system modeling, iii) configuring a system for the maximum net power output through design space exploration, iv) synthesis of feedback control tasks, and v) implementation.

Categories and Subject Descriptors: B.8.2 [**Performance and Reliability**]: Performance Analysis and Design Aids; C.3 [**Special-Purpose and Application-Based Systems**]—*Real-time and embedded systems*; J.7 [**Computers in Other Systems**]—*Real time*

General Terms: Design, Performance, Measurement

Additional Key Words and Phrases: Cyber-physical systems, Direct methanol fuel cell, Balance of plants system

ACM Reference Format:
Shin, D., Park, J., Kim, Y., Seo, J., and Chang, N. 2012. Control-theoretic cyber-physical system modeling and synthesis: A case study of an active direct methanol fuel cell. ACM Trans. Embedd. Comput. Syst. 11, 4, Article 76 (December 2012), 24 pages.
DOI = 10.1145/2362336.2362343 http://doi.acm.org/10.1145/2362336.2362343

1. INTRODUCTION

In cyber-physical systems (CPSs), computation is integrated with physical processes, with a tight linking and coordination between computational and physical resources. A pre-cursor generation of cyber-physical systems is to be found in areas as diverse as aerospace, automotive, chemical processes, civil infrastructure, energy, healthcare,

This work is supported by the Brain Korea 21 Project, National Research Foundation of Korea (NRF) funded by the Ministry of Education, Science and Technology (Nos. 20120005640 and 2012R1A6A3AO3038938). The ICT at Seoul National University provides research facilities for this study.
Authors' address: D. Shin, Dipartimento di Automatica e Informatica, Politecnico di Torino, Italy; J. Park, Y. Kim, J. Seo, and N. Chang, Department of EECS/CSE, Seoul National University, Korea; N. Chang (corresponding author); email: naehyuck@elpl.snu.ac.kr.

DOI 10.1145/2362336.2362343 http://doi.acm.org/10.1145/2362336.2362343

manufacturing, transportation, entertainment, and consumer appliances. The technical infrastructure of CPS, including methods and tools, must combine to bridge the gap between computational and physical resources. This infrastructure includes new programming languages and their integration with operating systems, new hardware and software components designed to improve performance and predictability, support for concurrency, and real-time networking [Lee 2006].

Model-based CPS development enables early integration of an entire system, followed by progressive replacement of computational models with physical components [Karsai and Sztipanovits 2008]. The specification of a CPS can be either structural and behavioral. Synthesis of the CPS generally starts from a behavioral specification, and is completed when the implementation matches the specification [Cheng 2006]. Existing model-based CPS synthesis techniques focus on the computational components [Zhang et al. 2008], and attempts to optimize a physical and a computational system together are hard to find. Conventional design techniques generally involve a fairly distant relationship between the physical system and computational system, implemented by structure such as system calls [West and Parmer 2006]. The specification of such an interface is intended to provide reliable functionality, while hiding the dependencies between components [Lin and Stankovic 2009]. Secure information exchange between the physical and computational system is one of the key concerns in designing a CPS [Dittrich and Haselkorn 2009; Anand et al. 2006].

The conventional design of a control system involves layer-by-layer optimization. For example, a vehicle engine generates higher power as more fuel and air are supplied. We can increase this mass flow by the introduction of a supercharger, with an impeller which is driven from the crankshaft. This increases the power output of the engine, but also draws mechanical power. The maximum net power output is unlikely to be realized by separation of the mass flow and the impeller speed. In a CPS, a balance-of-plant system (BOP) with more powerful actuators generally increase the response and efficiency of the physical system itself, but the actuators themselves require more power. Joint optimization becomes more difficult in modern CPS, in which the computational system is often very complicated. Nevertheless, Joint optimization of the physical system and computational system is a key factor in CPS synthesis.

In this article, we develop a practical CPS synthesis technique for an active direct methanol fuel cell (DMFC) system using a joint optimization concept. Neither the computational resources nor the BOP components are ideal. Characteristics such as response time, actuation range, and linearity are limited, and operating costs, including power consumption, should also be carefully considered. A conventional design may consider limitations of computational resources such as delay and word length [Eyisi et al. 2009] that affect physical system performance. However, the operating cost of the BOP system has often been neglected even though it can affect the efficiency of the entire CPS system. We introduce accurate actuator power models and characterize BOP components by real measurement to overcome the limitations of previous models.

A portable active DMFC system is a good example of a CPS in which the overall system efficiency should be optimized by a joint optimization of the physical system and the cyber world. The power output by a DMFC stack for a given rate of fuel consumption is greatly affected by the operating conditions, including methanol concentration, temperature of the stack, and cathode air velocity. An active DMFC system maintains the best possible operating condition in response to the environmental changes by the use of BOP system that includes pumps, blowers, and heat exchangers. An active DMFC and battery hybrid system architecture is viewed as a CPS in Figure 1. The physical system consists of a DMFC stack, a battery, power hybridization components, and a fuel system. The cyber world controller consists of BOP and the controller.

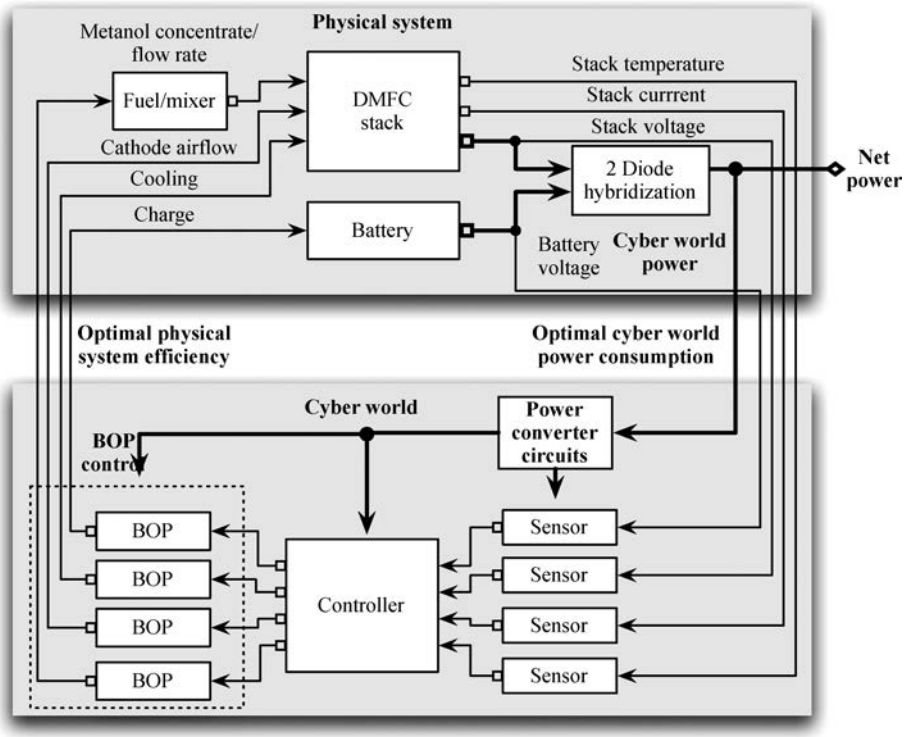

Fig. 1. Concept of the physical system and cyber world joint optimization of a portable active DMFC system.

As we describe in Section 6, a higher cathode air velocity results in a higher DMFC stack output power. In a typical laboratory setup, the cathode air pump is powered from the mains, and system optimization is mainly focused on the DMFC stack. However, the BOP components of portable DMFC must be powered by the DMFC stack. A lack of balance between the DMFC and the BOP system may significantly reduce the net power output, even if the stack output power is maximized. In particular, the extra power obtained from the DMFC stack becomes less than the extra power required by the blower if we increase its speed too much. The power gain from improving the BOP system may be offset by the power it consumes. The power consumption of each individual component is of course a lot smaller than the power generated by the DMFC stack, but the BOP components can consume more than 20% of the power generated by the stack [Chang et al. 2010]. Even the controller may consume more than 4% of the stack power depending on the operating condition. This makes it clear that the performance of the physical system and cyber world must be jointly optimized to achieve the maximum net power from the DMFC system as a whole.

We have developed a hardware and software platform on which to test our synthesis techniques. This platform includes a computing system, actuator controllers, a sensor interface, and power path circuits. The software platform provides a flexible architecture to support a range of control and communication tasks running in a real-time computing environment.

We model the whole DMFC system with Matlab Simulink and perform a design-space exploration to find the maximum net power output. We find the optimal operating point of the system, taking into account both the power generated by the DMFC stack and the power required to operate the BOP components. We synthesize cascaded feedback

control loop tasks that control the BOP system. We demonstrate a prototype implementation in which the outcome of this synthesis is used to implement a system based on our platform, and we evaluate its performance.

The rest of this article is organized as follows. In Section 2, we introduce the characteristics and design considerations of DMFC power systems. In Section 3, we present our CPS synthesis technique, which combines physical system and cyber world optimization in the content of a portable active DMFC. In Section 4, we give details the simulation models, and in Section 5, we describe the hardware and software platform. In Section 6, we present the result from our synthesis technique, and the result of implementation is described Sections 7. Section 8 concludes the paper.

2. ACTIVE DIRECT METHANOL FUEL CELL SYSTEM

2.1. Active Direct Methanol Fuel Cells

DMFC systems can be categorized into passive and active systems. Passive DMFC systems have no control systems making them good small portable power sources because of their compactness, reliability, and relatively low cost [Chan et al. 2008]. However, passive air breathing and fuel delivery are challenging because they are totally dependent on the operational environment [Qian et al. 2006; Chen and Zhao 2005].

Active DMFC systems can achieve a much higher power density than passive DMFC systems because they can operate much closer to the optimum condition, regardless of environmental changes, by the use of a BOP system that includes pumps, blowers and fans. BOP control is not cheap, but nevertheless active DMFCs are more cost-effective for generating larger amounts of power [Guo and Faghri 2006].

The performance of an active DMFC system is usually measured at its best operating condition in a laboratory. This is not realistic. For example, a feed pump is an essential BOP component. In a laboratory, a constant feed-rate peristaltic pump, which is accurate, pressure independent and stable, is typically used. However, a portable system cannot include such a large, heavy, complicated, and costly pump which requires continuous maintenance. A portable DMFC system requires a miniature BOP system, and the imperfect control that it provides largely determines the performance of the DMFC stack [Oedegaard and Hentschel 2006].

2.2. Control of Active Direct Methanol Fuel Cells

DMFC stacks require a very dilute methanol solution of around 1 Mol [Pei et al. 2006]. It is inefficient to carry such a weak solution because of its energy density. Therefore portable DMFC systems are fueled by neat methanol which is diluted to water within the system. In operation, the DMFC stack only consumes the methanol, and the exhaust contains the diluent, together with water produced by the chemical reaction. This can be condensed and reused. During this circulation process, some water will be lost and the need for a water supplement is a significant overhead for a portable system. Good water and fuel management are therefore essential [Blum et al. 2003].

The objective of the air flow control system is to supply sufficient atmospheric oxygen. At least 100ml/min of air is required for a 1W portable DMFC [Yang et al. 2006] in order to allow the stack to cope with an instantaneous demand for its load current [Vega-Leal et al. 2007]. In addition, a sufficient supply of oxygen to the cathode of the stack is necessary for efficient power generation. In a densely integrated active DMFC system, unlike a passive DMFC, the air supply strongly depends on the flow path. The BOP system must compensate for any obstruction or reduction in the performance of the air supply system to maintain the desired air flow. The efficiency of a DMFC system is also

affected by the temperature, which determines factors such as the stack performance, water reclamation, and the power consumption of the fan.

The BOP system, which is powered by the DMFC stack, is a significant power consumer. This power drain which can contribute to low efficiency, and so a portable active DMFC system should be efficient, beyond that required for a baseline passive DMFC system [Xie et al. 2002]. A higher flowrate pump and fan may increase the output of DMFC stack. But they may reduce the net power output of the DMFC system because their power consumption is proportional to the cube of flowrate.

2.3. Maximum Net Power Output

The net power considering effect of the BOP components can be expressed as follows:

$$P_{net} = P_{stack} - P_{BOP}, \tag{1}$$

where P_{net}, P_{stack} and P_{BOP} respectively are the net power output, the power generated by the stack, and the power consumed by BOP system.

A recent paper [Wishart et al. 2006] makes an effort to optimize the net power output of a proton exchange membrane fuel cell (PEMFC); this is a fuel cell that runs on hydrogen. The authors adopt existing models of a PEMFC, humidifier and cooling pump, and compressor, based on empirical data, and find the optimal temperature and stoichiometry using a genetic algorithm and simulated annealing. However, PEMFC BOP systems are considerably simpler than those of DMFCs because there is no need for a diluent circulation system or methanol concentration management. DMFC BOP system design and control is often neglected in the literature [Steele 2001]. We are aware of no systematic attempts at system integration and optimization which take the sensors and actuators as well as the computational components into consideration.

3. CPS SYNTHESIS FLOW

We propose a high-level synthesis technique for DMFC system design, as shown in Figure 2. We start with a system specification, including the parameter of the stack such as the area of the membrane, the number of stacked cells, the shape of the channels, and temperature constraints, as well as the target net power output. We determine the power converter specification, considering the electrical characteristics of the DMFC stack, the power requirement of the BOP components, and the required power output.

3.1. Characterizing BOP Components

We characterize the BOP components by making measurements. We measured the flowrate of the pumps and blowers with a flow meter while varying the supply current. From these results, we formulated accurate BOP power component models which are more realistic than previous models. The relation between power and flowrate is fitted by a polynomial, as described in Section 4.1. The dynamics of the actuators are recorded in a BOP component library. The parameters of the control tasks, including the period and proportional-integral (PI) control coefficients, are determined by the characteristics of the BOP components in the library. The control task model is described in Section 5.2.2. We built a Matlab simulation model of a whole DMFC system, including the stack and BOP components. Regarding on the range of the flowrates and pressure constraints, we can specify various types of pumps and blowers. The actual BOP models and DMFC stack parameters are determined from their specification and the BOP library. The simulation model enables us to verify the whole DMFC system so that we can explore the design space and consider various aspects of optimization.

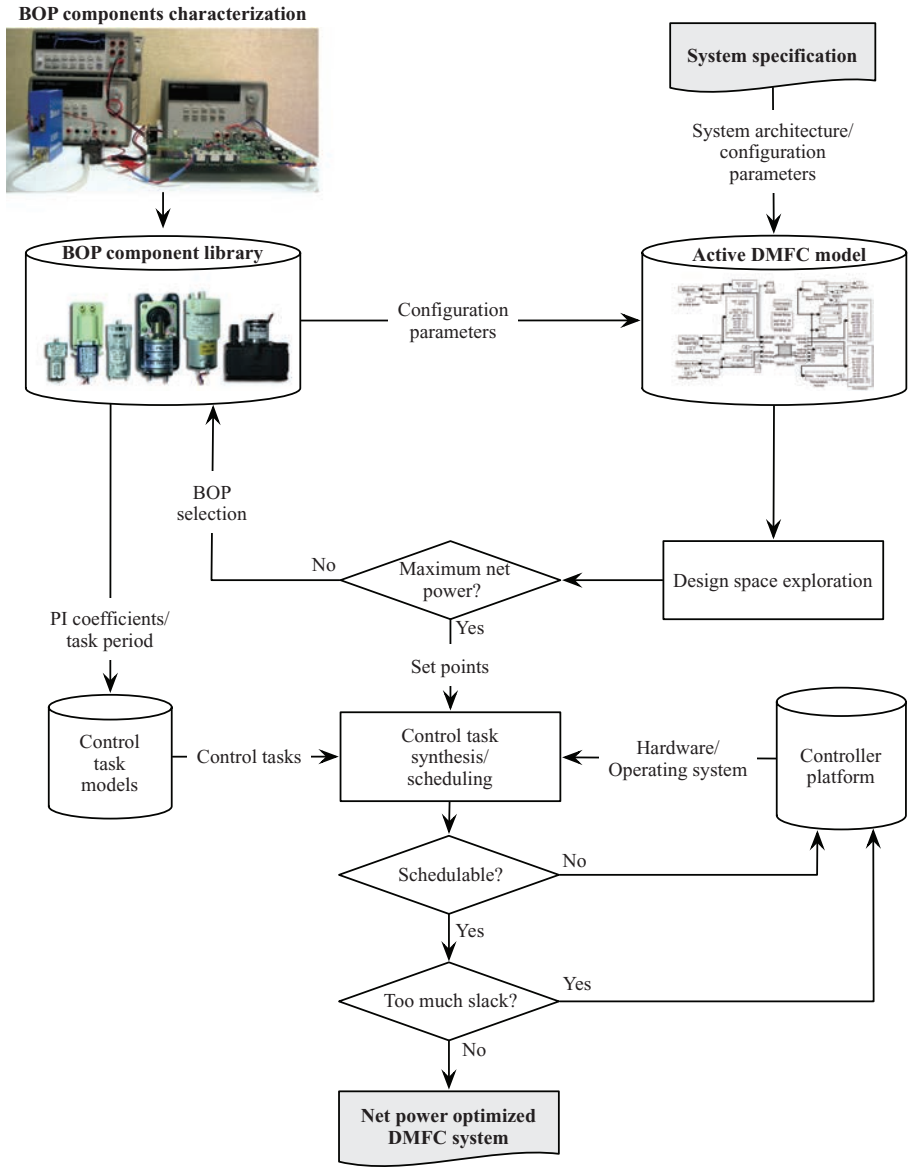

Fig. 2. Active DMFC system synthesis.

3.2. Hardware and Software Platform Design

The hardware platform includes components such as the low-pass filter for the ADC input, pump and blower drivers such as H-bridges, and DC-DC converters for the output. For DMFC system which outputs in the range of 20 to 200W, these circuits can be constructed from commercially available components which incorporate a reasonable amount of over-design. We have assembled a common platform to help DMFC system designers with chemistry or mechanical engineering background who may not able to build such a platform. The software platform runs a real-time operating system and control tasks implemented as cascaded feedback controllers, which are included in the

synthesis library. The system-level control algorithm is designed to operate the system safely and efficiently. Parameters such as period and feedback control coefficients are derived from the BOP component library and the operating conditions. We describe the controller platform in more detail in Section 5.

3.3. Physical System and Cyber World Joint Optimization

We seek the optimal operating point of the DMFC system considering the power generated by the stack and the power consumed by the BOP components, while maintaining the DMFC operating condition. The performance and power consumption of the cyber world including computing system and BOP are optimized to achieve this objective. If the maximum net power is not achieved by the current BOP component selection, we change the BOP components and explore design space again. We repeat these procedures until we achieve the maximum net power output. We explore the design space using Matlab Simulink. We synthesize cascaded feedback loop tasks to control the BOP. The system-level control algorithm is also tuned by using values from the synthesis. This optimization is described in more detail in Section 6.

3.4. Implementation and Verification

After exploring the design space, we finalize the set of BOP components, control tasks, and conditions for the system-level control algorithm. We verify the feasibility of this synthesis, including factors such as the schedulability of the control tasks on the platform. The performance required from the controller is determined by the specification of the actuators in the BOP system. A certain level of control quality must be provided by the BOP system to ensure safety. Operation of the BOP system must also protect the stack which is the most valuable component of in the system. The controller platform may or may not be able to provide the required performance. We change the BOP setup if the synthesized performance is not feasible with the controller platform; and we reduce the platform specification if it has too much redundant resource. We repeat these procedures until simulation confirms that we have an appropriate platform. Usually, the problem is to find a minimum platform specification to reduce the power consumption of the controller, because the full platform can provide sufficient computing power to control most active DMFC systems. We then integrate the DMFC system and complete a prototype. In Section 7, we describe system integration and prototyping, and present experimental results.

4. ACTIVE DMFC SYSTEM MODELING

CPS synthesis starts with the building of a component library, as described in Section 3.1. We now present models of the components of an active DMFC system, including the stack, heat exchanger, pump, and blower.

4.1. Pumps and Blowers

Pumps and blowers are fundamental components of many fluids systems. As our design objective is to maximize the net power output of a DMFC, our primary concern with these components is the relation between their power consumption and fluids flowrate. Pumps and blowers basically share the same model, even though they transport different fluids are different. Their power consumption is proportional to the pressure drop, which in turn determines flowrate of the fluid.

Existing design processes for portable fuel cells use simple models which relate power consumption to pressure drop and flowrate [Xue and Dong 1998; Wishart et al. 2006]. These pump and blower power models are variations of the following.

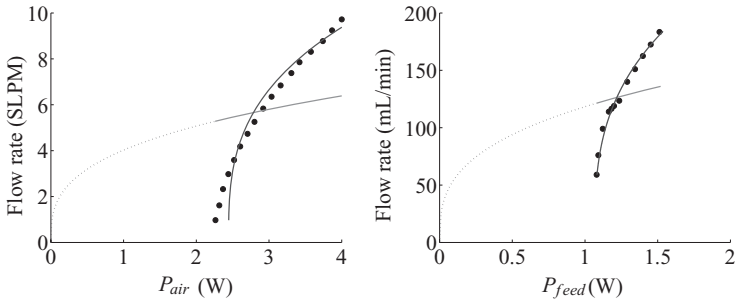

(a) Okenseiko RFP45B01R (b) KNF NF10-KPDC

Fig. 3. Power consumption of BOP pumps.

$$P_{pump} = \frac{\Delta P \dot{m}}{\eta}, \tag{2}$$

where $\dot{m}$ is the volumetric flowrate, and η is an efficiency constant. ΔP is the pressure drop, which can be expressed as,

$$\Delta P = k\dot{m}^2, \tag{3}$$

where k is a pressure drop coefficient determined by the component configuration [Xue and Dong 1998].

Portable DMFC systems, ranging from dozens to a few hundred Watts of net power output, use miniature pumps and blowers, which do not conform to the model above. We measured the power consumption of an RFP45B01R air pump from Okenseiko and an NF10-KPDC liquid pump from KNF and found that the power/flowrate curve is shifted along the power axis: very significant power is drawn when the flowrate is negligible. For example, the maximum power consumption of the NF10-KPDC is 1.53W, and the offset of 1.08W is unrelated to flowrate.

If we fit (2) to our measurements result, we obtain a huge error. The dots in Figure 3(a) and Figure 3(b) are our measurements; the gray dotted line is a fitted result with curve. The root mean square errors (RMSEs) of the RFP45B01R and NF10-KPDC are 4.023 and 3.306×10, respectively.

Pumps and blowers are driven by a DC motor, which is usually modeled as a linear system. The MATLAB library for fuel cell system simulation [Koegler and Kegelmeyer 2005] uses this type of model. But a DC motor has a nonlinear characteristic at low speeds [Kara and Eker 2004]. A DC motor needs to generate a certain amount of torque simply to overcome Coulomb friction. Thus, a dead-zone nonlinearity needs to be introduced in the pump model. Our pump model, which reflects the measured data, is as follows:

$$P_{pump,offset} = \frac{\Delta P \dot{m}}{\eta} + P_{offset}, \tag{4}$$

where P_{offset} is the offset power. If we fit this model to the measured data, the RMSEs of the RFP45B01R and NF10-KPDC data are 1.046×10^{-1} and 1.567×10^{-2}, respectively.

We surveyed a wide range of pumps and blowers that can be used for the portable DMFC systems for years. There are only a few products that satisfy our requirements for flowrate, power supply, chemical resistance, and durability. We measured the power consumption of ten miniature pumps of different types, including motor-driven, piezo-electric, and solenoid pumps. We assembled these BOP components with a DMFC stack

Table I. BOP Component Library Parameters

Type	Product	Manufacturer	Min flow (SLPM (air) or ml/min (liquid))	Max flow (SLPM (air) or ml/min (liquid))	k/η	P_{offset}(mW)
Air	RFP45B01R	Okenseiko	0.97	9.72	1.9	2444
	P09A03R	Okenseiko	0.71	3.88	31.6	565
	MAP-1004	Medo	0.20	0.91	808.4	228
	MAP-1104	Medo	0.07	2.38	103.2	342
	ML-6BS	Techno Takasuki	0.64	5.49	20.6	583
	CM-15-12	Sanwa Tsusho	0.34	1.53	295.2	295
Liquid	NF10-KPDC	KNF	60	180	7.538e-5	1067
Type	Product	Manufacturer	Max flow (ml/min)	Energy per stroke	Flow per stroke (μl)	
Liquid	SFM4	Thomas	63	340 mJ @ 12 V	300	
	030SP124-4TV	Bio-Chem Valve	0.96	225 mJ @ 12 V	4	
	SDMP306	Star	7	5.75 mJ @ 240 V	175	

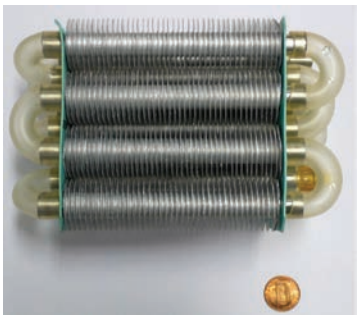

(a) Heat exchanger

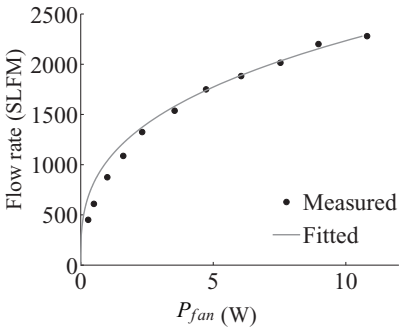

(b) Cooling fan power counsumption

Fig. 4. Heat exchanger and cooling fan characteristics.

and a heat exchanger to provide a real channel condition during the measurement process. We applied our power model to create a BOP component library. The parameters of models in this library are shown in Table I.

4.2. Heat Exchanger

The DMFC stack generates power and heat simultaneously. The amount of heat generated on the chemical reaction taking place, the heat output increases the temperature of the stack, which then affects the chemical reaction. A higher temperature enhance the reaction kinetics, but also increase the crossover of water and methanol. It turns out that the appropriate operating temperature for a stack is around 80℃ [Oedegaard and Hentschel 2006]. We need to maintain the temperature of the stack in a safe range as well as generating adequate power.

The heat exchanger to controls the temperature of the stack, as shown in Figure 4(a). It consists of fin-plated aluminum pipes and a cooling fan. We can change the thermal resistance between the stack and ambient air by changing the speed of the fan. The measured power consumption of the fan is shown in Figure 4(b). We also model the thermal resistance, thermal capacity of the stack, and radiator from their physical parameters. We calculate the cooling power needed to maintain the temperature of the stack close to 80℃. Figure 4(b) show the power consumption of the cooling fan at different flowrates.

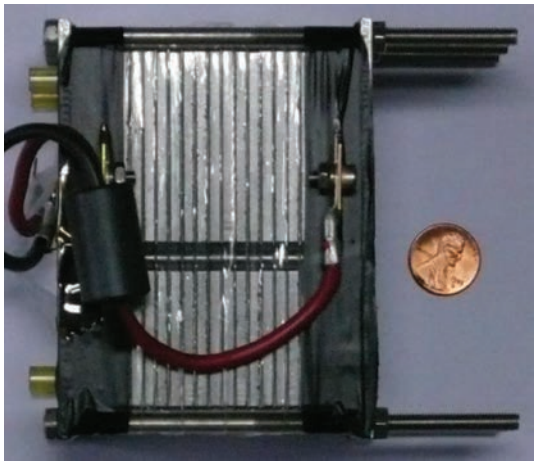

Fig. 5. DMFC stack.

4.3. DMFC Stack Model

We encountered numerous DMFC stack models in previous studies, including analytical models of the internal operation of a DMFC and equivalent circuit models representing the characteristics of a DMFC as an electrical power source [Scott et al. 1999; Wang and Wang 2003; Hsu et al. 2006]. Recent research has involved more complicated models which allow for multi-phase fluid dynamics and a 3D stack architecture [Liu and Wang 2007; Sun et al. 2009]. System-level design tools have also been developed. FClib, a Matlab/Simulink library for modeling and simulation of fuel cell systems is widely used [Turoni et al. 2005]. It contains well-defined simulation models of fuel cells, including the DMFC, verified through real applications.

We use the DMFC stack and peripheral models from the FClib library. We fit the parameters of those models to our DMFC, shown in Figure 5. This is a liquid-feed stack with 22 cells from Smart Fuel Cell. We measured the characteristics of this stack and selected the model parameters to match these characteristics. The concentration of the fuel is maintained at 1 Mol, and the cooling fan is controlled to keep the stack temperature below 80°C. Measured voltages and currents, and the resulting DMFC stack model are shown in Figure 6.

We also measured how the operation of the BOP affects the power output of the stack by varying the power supplied to the air and feed pumps at the same operating condition. Figure 7 shows the effects of air and fuel pump operation.

The voltage produced by a fuel cell can be expressed by the following equation:

$$V_{cell} = E_{thermo} - \eta_{act} - \eta_{ohmic} - \eta_{conc}, \tag{5}$$

where E_{thermo}, η_{act}, η_{ohmic}, and η_{conc}, respectively, are the thermodynamically predicted fuel cell voltage, the activation loss due to reaction kinetics, resistive losses from ionic and electronic conduction, and concentration losses due to mass transport. The activation losses are dominant in the low-current region, as shown in Figure 6(a), and the resistive losses are dominant in the intermediate region, as shown in Figure 6(b). Supply of fuel and air affect the mass transportation of the stack, and it results in the concentration loss in the high-current region, as shown in Figure 6(c). The concentration losses create a knee-point in the I-V curve of the stack, which effectively limits the output power of the stack.

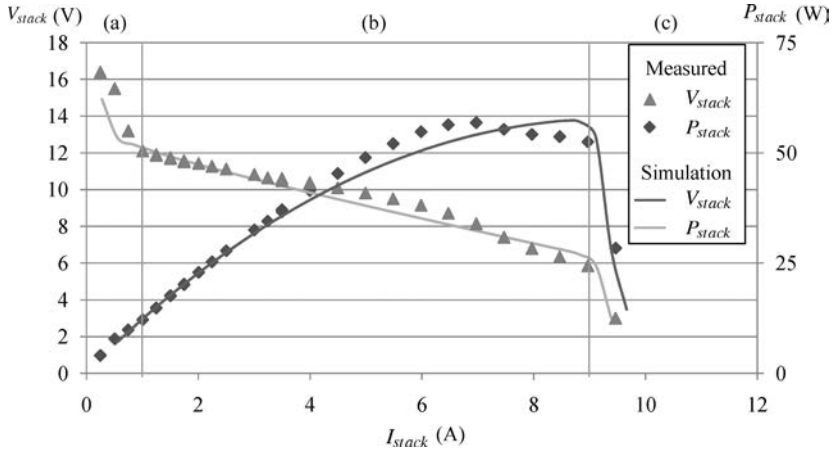

Fig. 6. DMFC stack voltage and current characteristic.

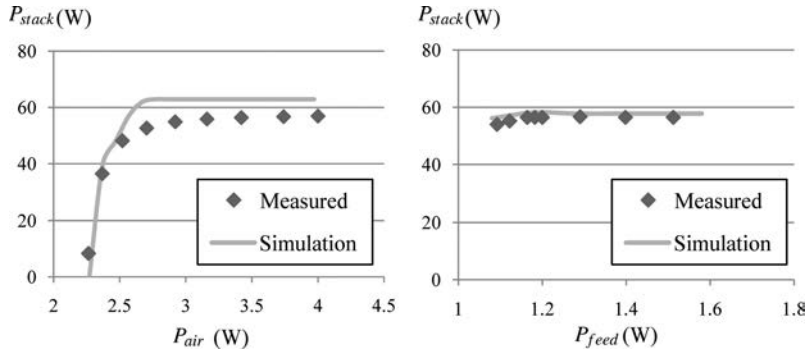

Fig. 7. DMFC stack power with different BOP power.

5. DMFC SYSTEM CONTROLLER PLATFORM DESIGN

We use the synthesis results to design a real system as described in Section 3. In this section, we introduce the hardware and software platform on which we implement this system. It allows us to explore the design in pursuit of a holistic optimization. The platform is intended to have a flexible and scalable architecture that can meet various system requirements. The software platform is based on a real-time OS with an interrupt-based multi-task architecture.

5.1. Hardware Platform Design

5.1.1. Computing System. DMFC control requires (i) a powerful computing capability, (ii) a rich set of embedded peripherals, such as analog-digital converters (ADCs), digital-analog converters (DACs), timers, and pulse-width modulators, (iii) software and operating system compatibility, (iv) support for standard communication protocols, and (v) high reliability.

A single-chip microcontroller is simple and economical. Manufacturers such as Freescale and Texas Instruments produce 32-bit microprocessors with embedded peripherals which allows a controller to be designed with as few off-chip components as possible. The PowerPC 555 is a particularly well-known example; it runs at 40MHz and has previously been used for DMFC system control [Heideck et al. 2004]. We use

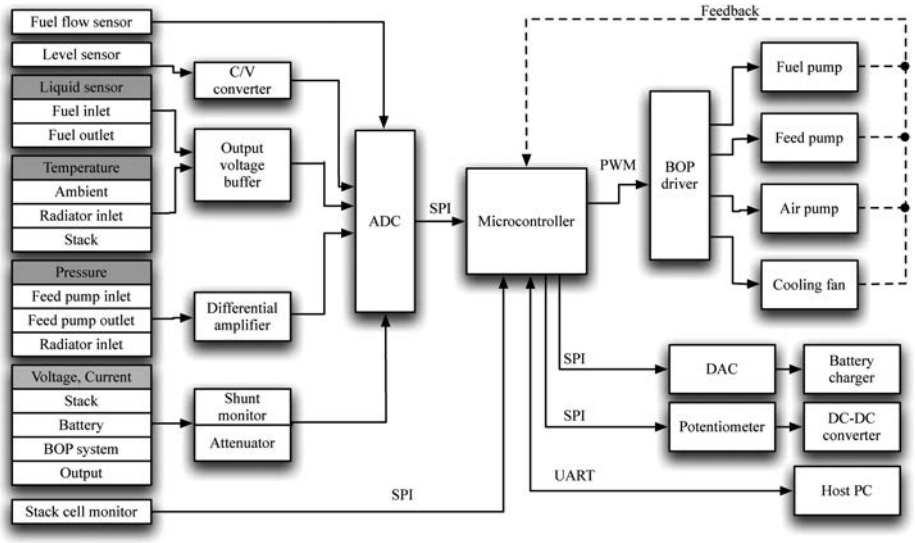

Fig. 8. Hardware platform architecture.

the Texas Instruments TMS470 microprocessor, which has a 32-bit ARM7 core running at 60MHz.

5.1.2. Measurement. The output from the sensors in the DMFC system require appropriate signal translation circuits. We use capacitance-voltage converters, output voltage buffers, differential amplifiers, together with level, temperature, and pressure sensors. In practice, it is more difficult to measure voltage and current than other quantities due to their high-frequency characteristic. We accommodate this with a low-pass filter with a fine-tuned cutoff frequency in front of the measurement circuit.

5.1.3. BOP Component Drivers. The actuators used in an active DMFC BOP system include heterogeneous types of pumps, blowers and fans. Actuators may be driven by DC motors, solenoids, or piezoelectric transducers. We use a general full-bridge driver with four transistor switches for the BOP drivers shown in Figure 8. This driver is capable of running a motor in both directions as well as applying active braking.

A cost-effective choice of drivers depends on the control policy. For example, a fan does not have to change speed quickly or run in reverse, so we can use a low-side driver to implement its feedback control loop. But the pump for methanol delivery needs to achieve a faster response and PI control requires a relatively large value of the proportional constant. This response can involve instantaneous reversing of the motor current, and so a full-bridge driver is needed. We use a full-bridge driver for to control the pumps because they requires elaborate control to maintain the required flowrate.

5.1.4. Power Path Circuit. We designed the power path circuit using diode-OR switches, DC-DC converters and a battery charger, as shown Figure 9. The fuel cell and battery power hybridization architecture based on a two-diode connection was introduced in Kim et al. [2010]. The output voltage is regulated by the DC-DC converter (ⓐ). Each power source is connected through a diode (ⓑ), and thus only the power source with the higher terminal voltage is connected to the DC bus (ⓒ) at any time, while the diodes prevent reverse current flow from one source to the other. We use a battery connected to a charger (ⓓ) to allow the DMFC stack to run at a constant current, even if the load changes. We achieve constant-current operation by varying the battery charge current

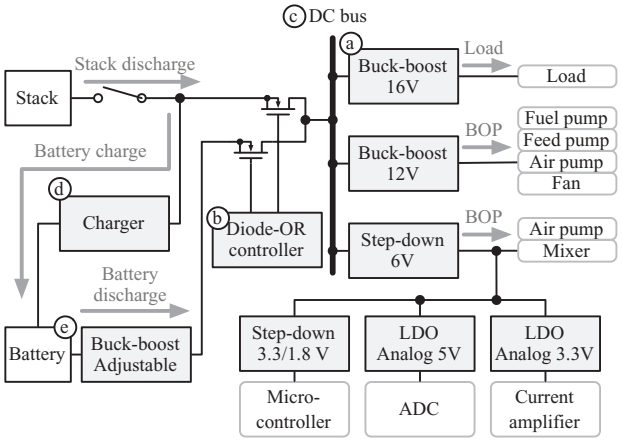

Fig. 9. DC power distribution path and power-up sequence. Circled numbers denote the order in which components are enabled.

to match the load current. The lower limit of the stack voltage can be adjusted by the output regulator of the battery (ⓔ).

We have already explained that components such as pumps, fans, and sensors require different supply voltages. In addition, a computing system requires different supply voltages for its core and I/O sections. The output voltage required from the DMFC system may also vary from application to application. Therefore, an active DMFC system has to provide several different DC voltages by means of heterogenous DC–DC converters as shown in Figure 9.

We use a MOSFET diode-OR such as the LTC4355 from Linear Technology to minimize the diode loss. This diode-OR measures the voltages at its two input terminals, and only closes the switch that is connected to the higher voltage. This eliminates the power loss induced from the diode forward voltage drop, except for the short periods during which the MOSFET is changing its input.

5.2. Control Software Platform

5.2.1. Control Software Architecture. Simple timer-based control tasks without an RTOS are not suitable for modern active DMFC systems. A large number of such tasks rapidly become unmanageable as communication and monitoring functions are swamped. Most RTOSs also offer support for (i) task scheduling, (ii) runtime library, (iii) communication protocol stacks, (iv) device drivers, and (v) a software development environment, with other convenient features for developing embedded systems.

Figure 10 shows the architecture of the DMFC control software. The inputs to the software are signals from the sensors, and its outputs are signals to control the actuators. The control software is composed of multiple real-time tasks, including sensor input, actuator output, analog-to-digital and digital-to-analog conversions, feedback and feedforward control loops, and system management. These tasks communicate through a shared memory and synchronized communication channels such as message queues.

The I/O task is responsible for processing input from and sending output to BOP components, the user interface, and the host computer, which do not receive direct communication from any other task. I/O needs to be jitter-free for reliable control, and therefore the I/O task has the highest priority. The physical layer of the I/O task

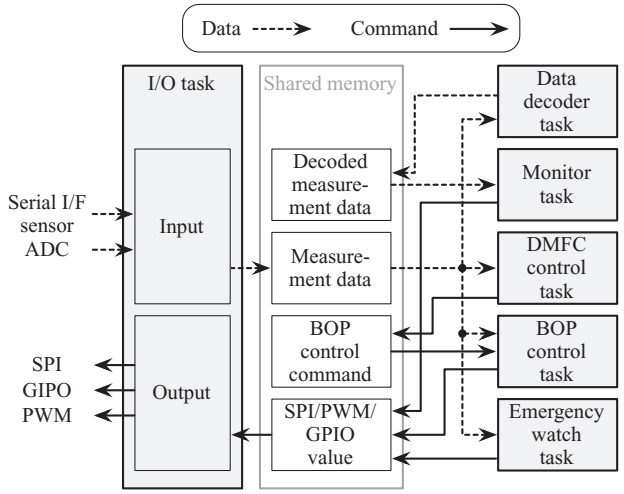

Fig. 10. Software block diagram and control/data flow.

provides device-dependent communication with ADCs, DACs, and general-purpose input and output (GPIO) ports.

The I/O task stores its raw input values in a shared memory. A separate data decoder task converts the integer values received from ADCs into meaningful floating-point values in appropriate units. The use of a single I/O task prevents floating-point conversions being repeated by multiple tasks. Other tasks may use either the raw or converted values; the control tasks mainly use raw integer values for computational efficiency.

The control tasks are responsible for tasks such as stack management, stack and battery power balancing, and fuel concentration and temperature management. The control tasks read input data from, and write control data back into, the shared memory. The execution times of control tasks may vary with the system state, but jitter should not occur by guaranteeing that the worst-case execution times are shorter than the period of the I/O task. Multiple cascaded feedback and feedforward control loops for each pump and fan are implemented in the control tasks. Control constants such as the proportional and integral constants, and the I/O period, are obtained from our exploration of the design space.

If exceptional conditions occur, such as an unacceptable methanol concentration or an excessive temperature, an emergency watch task immediately performs a predefined turn-off sequence. This may include opening the stack switch, flushing fuel from the stack, and cooling the stack. This watch task has a high priority so that it can protect the system as quickly as possible.

The monitor task interfaces the controller with the user's host computer. The user can utilize this task to change BOP variables, alter the operating policy, or read ADC values.

5.2.2. BOP Feedback Control. DMFC systems are subject to various disturbances, and the operation of BOP components should be made robust to such environmental disturbances by feedback or feedforward control. Operating the fuel pump with an open-loop control does not achieve a constant methanol supply rate because the flowrate of the methanol is dependent not only on the frequency of pulse-width modulation (PWM) signal, but also on the liquid composition and the pressure at the pump. So we use feedback to compensate for these factors, as shown in Figure 11.

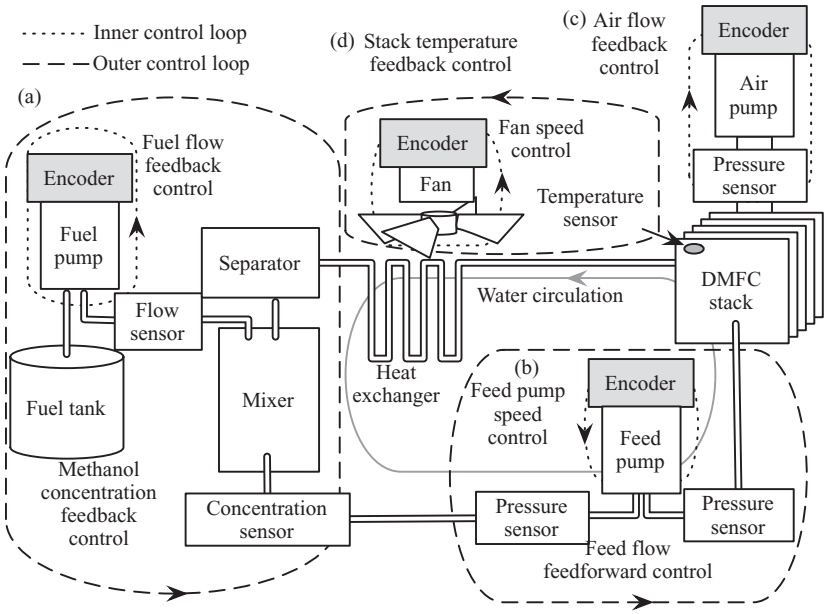

Fig. 11. Generic active DMFC BOP system architecture.

In general, single-loop feedback can achieve stable operation when there is not much measurement delay. However, plastic tubing connecting the components of the fuel cell has elastic walls, it acts as an accumulators, so that a change in the pump speed does not immediately affect the flowrate. If we only measure the flowrate, there is significant measurement delay which may make a single-loop feedback control unstable. In contrast, a cascaded feedback control performs well in such a situation. As shown in Figure 11, we use an inner feedback loop to compensate for the measurement delay of the outer loop.

In the inner feedback loop, at time t, we determine the frequency of PWM $f(t)$ that controls the pump speed as follows:

$$f(t) = f_{sp} + P_f e_\omega(t) + I_f \int_0^t e_\omega(t)dt,$$

where f_{sp} is the set-point PWM frequency, $e_\omega(t)$ is the error in measuring the pump speed, and P_f and I_f are the P and I coefficients of the inner PI feedback controller. We determine the rotational speed $\omega(t)$ of the fuel pump in the outer feedback loop required to achieve a desired flowrate in the cascaded control loop as follows:

$$\omega(t) = \omega_{sp} + P_\omega e_{flow}(t) + I_\omega \int_0^t e_{flow}(t)dt,$$

where ω_{sp} is the set-point rotational speed, $e_{flow}(t)$ is the error in the flowrate, and P_ω and I_ω are the P and I coefficients of the outer feedback controller.

The flowrate of the feed pump is much higher than that of the fuel pump, and thus we may use a diaphragm pump, but the flowrate of this sort of pump is significantly affected by the pressure difference between the inlet and outlet. However, this change in flowrate has been measured by the manufacturer and is specified on a datasheet. Therefore, we can employ feedforward control of the feed pump, consisting of an inner

feedback loop and an outer feedforward loop, shown as Figure 11. The use of feedforward allows to do without a complicated flow sensor. The feedforward loop controls the motor speed ω_{motor} based on the pressure measurement of the outer loop as follows:

$$\omega_{motor} = a(P_{outlet} - P_{inlet}),$$

where P_{inlet} and P_{outlet} are the inlet and outlet pressure, respectively. The value of $a > 0$ is empirically determined to mitigate the impact of the pressure difference on the flowrate. The inner feedback loop that controls ω_{motor} is identical to that used for controlling the fuel pump. However, we used an NF 5 RPDCB-4 pump, which has an embedded rotational speed controller, rather than a separate encoder.

The air blower supplies air including oxygen to the stack as illustrated in Figure 11. Insufficient oxygen will obviously reduce stack performance; but running the air pump too fast wastes power [Scott et al. 1999]. The flowrate of an air pump in its low-pressure range is a function of the pressure across the pump. We can measure this with pressure sensors, as shown in in Figure 11(c). The major external factors affecting control of the airflow are constrictions of the air path due to foreign bodies such as dust on the filter or a partial blockage.

The feedback loop in Figure 11(d) maintains the temperature of the stack by controlling the speed of the cooling fan. There is an IC available that provides temperature control with a fan. It can generate the PWM signal to drive a fan to maintain a defined temperature or runs the fan at a speed programmed by a microprocessor.

5.2.3. Power Path Control. Another important task is controlling the electrical operating condition of the DMFC stack. The use of battery hybridization allows the stack to run at a constant current as far as possible while the system as a whole the load current changes to accommodate[Kim et al. 2010]. The battery charging current and clamp DMFC stack voltage are controlled by the two-diode circuit. We measure the stack current periodically and adjust the battery charge current to return the stack current to a its optimal value. The battery charge current is controlled by a software feedback controller. The DMFC stack and Li-ion battery dynamics were determined through a step response analysis. The battery charge current $I_{chg}(t)$ at time t can be expressed as follows:

$$I_{chg}(t) = I_{chg_{sp}} + P_{chg}e_{chg}(t) + I_{chg}\int_0^t e_{chg}(t)dt,$$

where $I_{chg_{sp}}$ is the charge current set-point, $e_{chg}(t)$ is the error at t, and P_{chg} and I_{chg} are the P and I coefficients of the PI controller.

The battery drains when the load demand exceeds the capacity of the DMFC stack. The maximum power obtainable from the stack is determined by the clamping voltage V_{clamp} of the two-diode circuit. The voltage-current (V-I) characteristic of a DMFC stack is affected by many factors such as temperature, methanol concentration, and air supply. Thus the V-I curve of the DMFC stack may move up and down, even if V_{clamp} is kept constant. We resolve this problem by adjusting the DC–DC converter output voltage V_{clamp} to track the voltage of the DMFC stack. This is performed by a task on the microprocessor that controls the DC–DC converter output voltage. It sets the battery voltage V_{clamp} to the stack voltage measured when $I_{stack} = I_{target}$, is that

$$V_{clamp} = V_{stack}|_{I_{stack}=I_{target}}.$$

This task does not need to be run frequently because the performance of the stack does not change rapidly. It is hard to obtain the V-I characteristic of a DMFC stack as a function of the various external factors. Therefore, we fine-tune the control coefficients and assume that the operating environment changes very slowly.

5.2.4. System Operation Control and Protection. As well as operating the BOP system and the power-path circuits at the desired operating point, we need to make the necessary system-level control decisions for a safe and reliable operation of the DMFC system. The system-level control algorithm for the active DMFC systems decides the time to perform at least four operations: start up, preheating, air depletion and shut down.

It is necessary to maintain the charge on the battery within a certain range in order to sustain the constant-current operation of the stack in a stand-alone DMFC system. Thus the battery is charged whenever the load current is smaller than the stack current. We temporarily shut down the stack when the battery is fully charged, and resume operation when the charge on the battery drops below a threshold.

The DMFC stack cannot start up and or shut down instantaneously. Furthermore, it is inefficient until it reaches to its operating temperature. The difference between the nominal DMFC stack efficiency and its efficiency during start-up and shut-down is an important aspect of a DMFC. This factor determines the maximum load current and the minimum battery capacity, which in turn affects the total volume, weight, and cost of the system.

It is important to reach the correct operating temperature as quickly as possible. Most portable DMFC systems are not equipped with an external heater, and thus an efficient operating temperature is only achieved by the stack relying on the heat generated by its own operation. The amount of heat generated by the stack is mainly determined by its internal resistance. We control the power path to adjust the operating current and voltage. Under given conditions, particularly ambient temperature, preheating the DMFC stack to its operating temperature only requires a small amount of energy, and significantly improves system efficiency. Our system reduces the preheating time by keeping the stack output power as high as possible when start up.

Stack efficiency is gradually drops over time, due to aging caused by ions and particles adhering to the membrane, fuel, and air channels. Air depletion is one way to mitigate this problem. This involves periodically stopping the air supply at a frequency and for a duration that depends on the DMFC characteristics. In our system, we perform air depletion when the voltage drops below a certain threshold after the stack reaches its constant current operating condition.

The flowchart in Figure 12 shows the behavior of our system-level control algorithm, which concurrently controls the behavior of the feedback control tasks and the hybrid-power path control task. In particular, this algorithm starts or terminates the control tasks and determines the objective of the feedback control using data obtained by monitoring the system status, including the charge of the battery, the demand load, and temperature.

The control algorithm initiates the BOP components and control tasks. Safe start-up of DMFC stack operation requires the BOP components to the waken up in a particular sequence. Typically the fuel pump is first, followed by the air blower, the injection pump, and the cooling fan. If the temperature of the stack T_{stack} is lower than the operating point $T_{operation}$, we increase the DMFC current I_{stack} by dropping the two-diode clamping voltage V_{clamp} until the power from the DMFC P_{stack} reaches its knee-point. At the knee-point, P_{stack} does not increases with I_{stack} because of the drop in stack voltage. The DMFC stack is connected to the power-path circuit when the temperature of the stack, I_{stack} and V_{clamp} correspond to the target operating condition. After reaching this condition, we perform the air-depletion process to recover the stack performance. This involves disconnecting the DMFC stack, stopping the air blower, restarting the air blower, and reconnecting the DMFC stack. DMFC operation is terminated by turning off the BOP components when the battery is fully charged. The time to restart the DMFC is determined by the charge on the battery and the demand load.

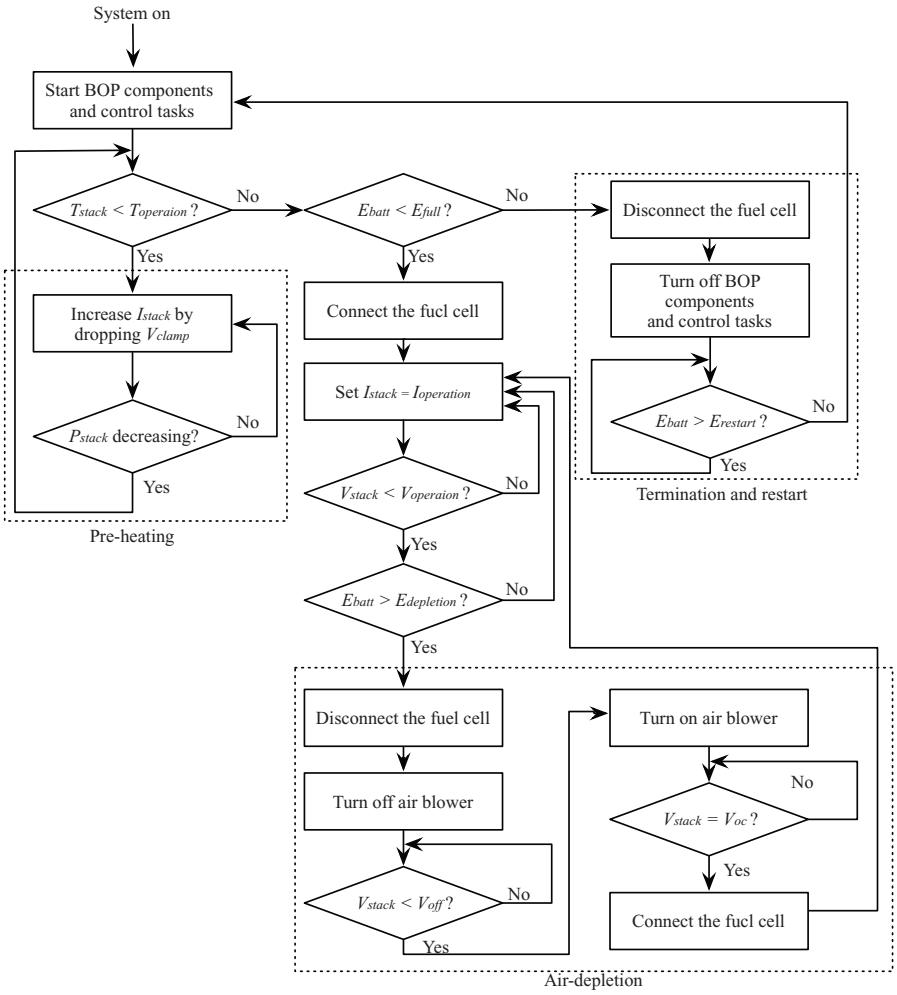

Fig. 12. Algorithm for system-level control.

6. PHYSICAL SYSTEM AND CYBER WORLD JOINT OPTIMIZATION

We propose a systematic CPS synthesis process which jointly optimizes the physical system and the cyber world. We have applied this synthesis technique to maximize the net power output of an actual DMFC. We performed an optimization to obtain the operating point of the system using a system-level simulation with component models built from real measurements. The system behavior, including the DMFC stack start-up and shut-down conditions, is determined by the operating point.

We composed an integrated DMFC system model, including stack, pumps, blowers, and heat exchanger, as shown in Figure 13. We assumed that the ambient air temperature is 300K, and supply a 1 Mol methanol solution to the stack. We changed the flowrate and the cooling capacity by adjusting the power supplied to the pumps and the cooling fan. The simulation was repeated until the operation of the DMFC stack status converged to a steady state. We simulated the operation of the stack at different

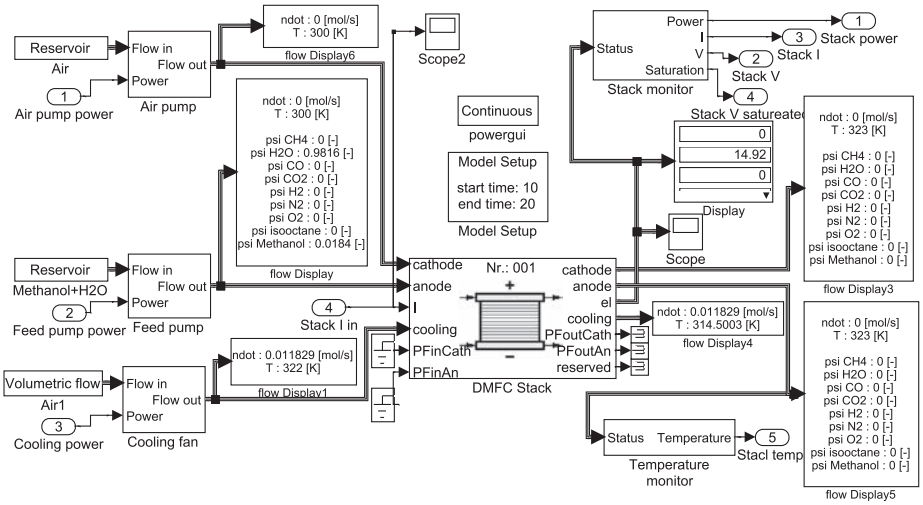

Fig. 13. DMFC system simulation setup using FClib.

air and fuel flowrates, and calculated the fan power required to cool the stack to keep its temperature under 80℃.

We can estimate the overall system efficiency by considering the power consumption of the BOP components P_{BOP}. Their net power is given by (1), and we can determine P_{BOP} as follows:

$$P_{BOP} = P_{fuel} + P_{feed} + P_{air} + P_{fan}, \tag{6}$$

where P_{fuel}, P_{feed}, P_{air}, and P_{fan} respectively are the power consumption of the fuel pump power, feed pump, air pump, and cooling fan.

Figure 14 shows the net output power for different amount of power consumed by the BOP components. The surface is not convex but contain the globally optimal operating point. Air supply can be a bottleneck when insufficient power is supplied to the air pump. In this situation, the stack power output is limited by the concentration loss with. The feed pump can produce a similar phenomenon, but its influence is relatively small. If there is sufficient air and fuel, the temperature of the stack increases, and so it has to be cooled by the heat exchanger. We need to adjust power supplied to the cooling fan to meet the collect temperature. The design surface has a complicated shape in this region because the temperature of the stack is affected by the air and fuel supply and not just the amount of cooling.

The pump power model without P_{offset} tends to underestimate the power consumption. If enough air and fuel are supplied, the stack power does not increase beyond a certain point, which is determined by the fuel concentration even if more air and fuel are supplied. Therefore the optimal net power can be found at the point at which the pumps supply enough air and fuel for the minimum power consumption. If the pump power is underestimated, the optimization will converge to an air and fuel supply with less power. Figure 14(a) and Figure 14(b) show the effect of P_{offset} on the optimal operating point. The estimated net power output at (a) is 56.45W, and at (b) it is 55.27W.

We performed the same experiment with a different air blower, the P09A03R from Okenseiko, which is only marginally able to supply sufficient air to saturate the DMFC stack. Equation (2) overestimates the power consumption in this case. As a result, the

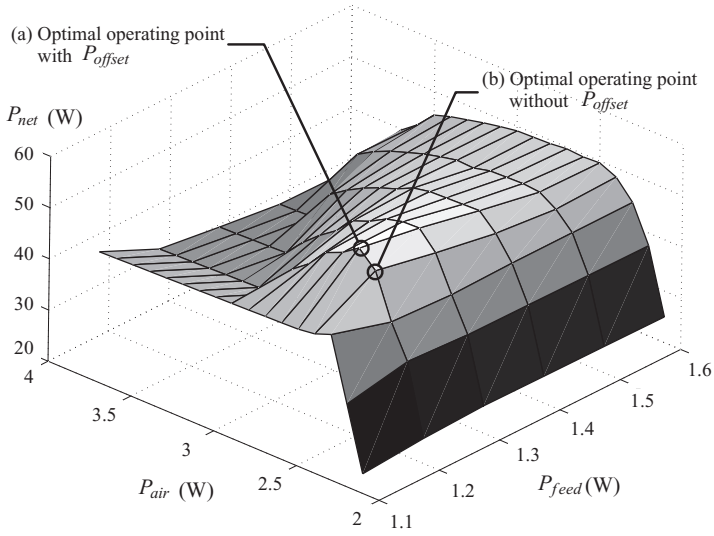

Fig. 14. Exploring the design space to achieve for the maximum net power of the DMFC system with an Okenseiko RFP45B01R blower.

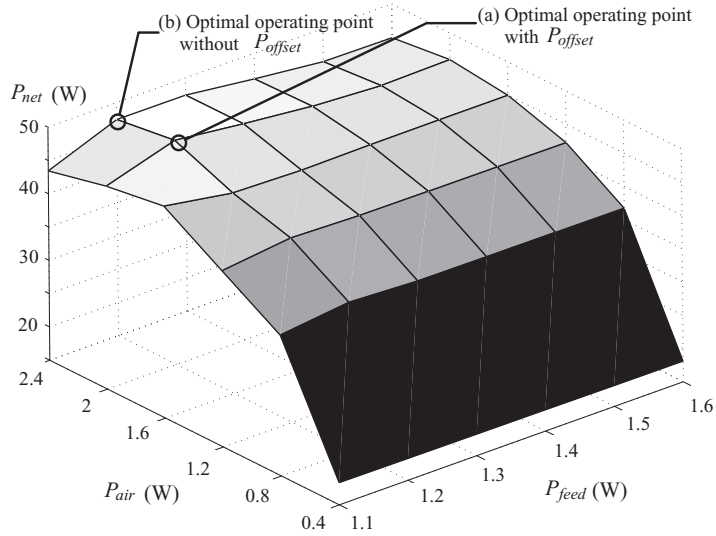

Fig. 15. Design space exploration for the maximum net power of the DMFC system with Okenseiko P09A03R.

optimal value of P_{air} is larger than the optimal P_{air} derived using (4), as illustrated in Figure 15. The net power at (a) is 52.26W and at (b) it is 50.92W.

7. PROTOTYPING AND EXPERIMENTAL RESULTS

We implemented a prototype DMFC system to verify the proposed synthesis framework. Figure 16 shows the integrated DMFC system including the stack, pumps, heat exchanger, and controller board. We integrated this system with the mixer, separator, and filters used in the EFOY1200 DMFC system from Smart Fuel Cell. The integrated fuel mixer and gas-liquid separator consists of a fuel filter, a fuel chamber, a gas-liquid

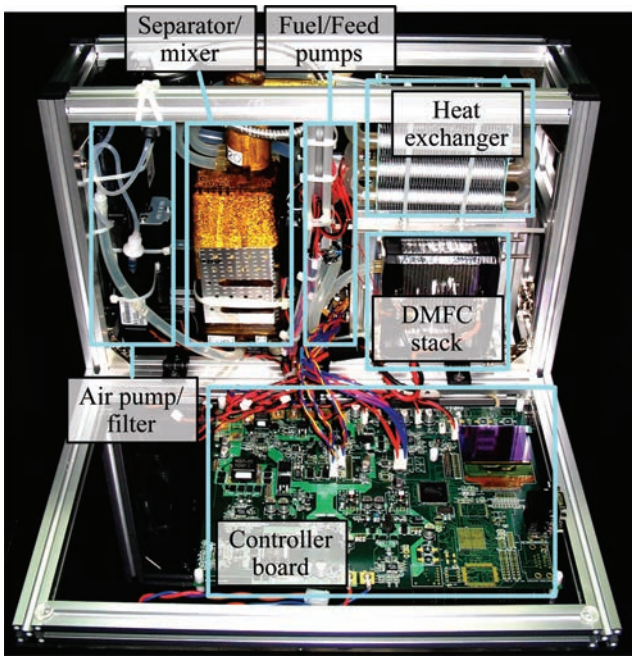

Fig. 16. Implemented DMFC system prototype.

Table II. Prototype Features

Component	Product	Manufacturer	Operating point	
			flowrate	Power
Fuel pump	SMF-4	Thomas	0.04ml/min	0.04W
Feed pump	NF10-KPDC	KNF	116.5ml/min	1.18W
Air pump	RFP45B01R	Okenseiko	5.56l/min	2.77W
Cooling fan	9G0812H102	Sanyo Denki	1920SLPM	6.4W

separator, and a vapor recovery structure. All of these components are made from polycarbonate.

The hardware controller platform that we developed contains measurement circuits, BOP drivers, and DC-DC converters to operate the DMFC. It can apply feedback control to the BOP components and operate the DMFC stack at constant current. We also wrote the controller software, which runs on a real-time operating system. The software controller accept the synthesis results as a parameter.

We selected BOP components from the library, and determined their operating points from the result of design space exploration. Selected BOP components and their operating points are shown in Table II. We operated the system at this point, and measured its performance. Figure 17 shows the power consumption of each component in the system. The average power generated by the DMFC stack was 56.45W. The fuel pump, feed pump, air pump, and cooling fan respectively consumed 0.04W, 1.28W, 2.77W, and 6.4W.

The dominant power consumer is the cooling fan, and its power consumption depends on the system operating condition. If a condition such as ambient temperature changes, then the optimal operating point also changes.

Another concern is the long-term effect of the operating condition on the DMFC stack. The stack is the most valuable part of the DMFC. Therefore, we need to maximize its

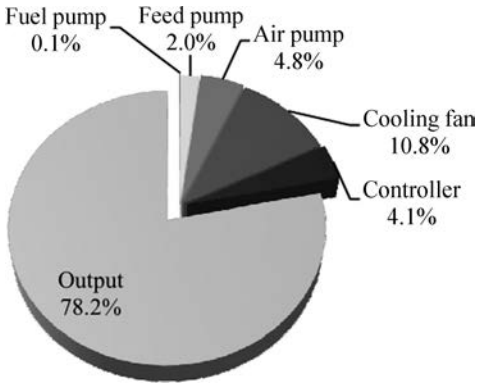

Fig. 17. Destination of the power generated by the stack in our prototype DMFC system.

lifetime while maintaining its performance. We have used the system power output as our objective, but this could be replaced by the another objective.

8. CONCLUSIONS

Cyber-physical systems require seamless integration between the physical system and cyber world, but there may be an appreciable discrepancy between theory and practice; limitations in the interface between the physical and cyber resources are a primary cause of such a discrepancy.

In the portable DMFC system introduced in this article, sensors, pumps, blowers, and the power path circuit are tightly combined with software control. It can regarded as a sensor-based autonomous system which is a representative example of a CPS. The challenge that we address is to design a practical CPS synthesis flow for a portable hybrid power supply system by joint optimization of the physical system and cyber world. We have shown how a whole DMFC can be optimized systematically.

We performed a system modeling, design-space exploration, synthesis and implementation of a DMFC. Initially, we maximized net power within the trade-off between DMFC stack efficiency and BOP power consumption. We modeled the whole DMFC system with Matlab Simulink and explored the design space to find the operating point corresponding to the maximum net power output, while simultaneously considering the power generated by the DMFC stack and the power required to maintain the DMFC operating condition. We designed hardware and software controller platforms with sufficient computing power for active DMFC systems. We defined operating procedures for the DMFC system to guarantee its safe operation. The behavior of the cyber world, including computing system and BOP components, are optimized to achieve this objective. Finally, we demonstrated a prototype implementation. We implemented a DMFC system based on the outcome of our synthesis on the our platform architecture and measured its performance.

REFERENCES

ANAND, M., CRONIN, E., SHERR, M., BLAZE, M., IVES, Z., AND LEE, I. 2006. Security challenges in next generation cyber physical systems. In *Proceedings of Beyond SCADA: Cyber Physical Systems Meeting (HCSS-NEC4CPS)*.

BLUM, A., DUVDEVANI, T., PHILOSOPH, M., RUDOY, N., AND PELED, E. 2003. Water-neutral micro direct-methanol fuel cell (DMFC) for portable applications. *J. Power Sources 117,* 1-2, 22–25.

CHAN, Y., ZHAO, T., CHEN, R., AND XU, C. 2008. A small mono-polar direct methanol fuel cell stack with passive operation. *J. Power Sources 178,* 1, 118–124.

CHANG, N., SEO, J., SHIN, D., AND KIM, Y. 2010. Room-temperature fuel cells and their integration into portable and embedded systems. In *Proceedings of the Asia South Pacific Design Automation Conference (ASP-DAC)*. 69–74.

CHEN, R. AND ZHAO, T. 2005. Mathematical modeling of a passive-feed DMFC with heat transfer effect. *J. Power Sources 152*, 122–130.

CHENG, A. M. K. 2006. Synthesis, verification, and optimization of cyber-physical systems. In *Proceedings of the NSF Workshop On Cyber-Physical Systems: Research Motivation, Techniques and Roadmap*.

DITTRICH, D. AND HASELKORN, M. P. 2009. Visualizing secure cyber-physical systems. In *Proceedings of the Workshop on Future Directions in Cyber-physical Systems Security*.

EYISI, E., PORTER, J., HALL, J., KOTTENSTETTE, N., KOUTSOUKOS, X., AND SZTIPANOVITS, J. 2009. Panecs: A modeling language for passivity-based design of networked control systems. In *Proceedings of the 2nd International Workshop on Model Based Architecting and Construction of Embedded Systems (ACES-MB)*.

GUO, Z. AND FAGHRI, A. 2006. Miniature DMFCs with passive thermal-fluids management system. *J. Power Sources 160,* 2, 1142–1155.

HEIDECK, G., PURMANN, M., AND STYCZYNSKI, Z. 2004. Micro-computer control for a fuel cell test bench for residential use. *J. Power Sources 127,* 1-2, 319–324.

HSU, N.-Y., YEN, S.-C., JENG, K.-T., AND CHIEN, C.-C. 2006. Impedance studies and modeling of direct methanol fuel cell anode with interface and porous structure perspectives. *J. Power Sources 161,* 1, 232–239.

KARA, T. AND EKER, I. 2004. Nonlinear modeling and identification of a dc motor for bidirectional operation with real time experiments. *Energy Conversion Manage. 45,* 7-8, 1087 – 1106.

KARSAI, G. AND SZTIPANOVITS, J. 2008. Model-integrated development of cyber-physical systems. In *Proceedings of the 6th IFIP WG International Workshop on Software Technologies for Embedded and Ubiquitous Systems*. Springer-Verlag, Berlin, 46–54.

KIM, Y., SHIN, D., SEO, J., CHANG, N., CHO, H., KIM, Y., AND YOON, S. 2010. System integration of a portable direct methanol fuel cell and a battery hybrid. *Int. J. Hydrogen Energy 35,* 11 (June), 5621–5637.

KOEGLER, W. S. AND KEGELMEYER, W. P. 2005. *FCLib: A Library for Building Data Analysis and Data Discovery Tools*. Vol. 3646/2005. Springer, Berlin.

LEE, E. A. 2006. Cyber-physical systems - are computing foundations adequate? In *Proceedings od the NSF Workshop On Cyber-Physical Systems: Research Motivation, Techniques and Roadmap,*.

LIN, S. AND STANKOVIC, J. A. 2009. Performance composition for cyber physical systems. In *Proceedings of the Ph.D. Forum of the 30th Real-Time Systems Symposium (RTSS'09)*.

LIU, W. AND WANG, C.-Y. 2007. Three-dimensional simulations of liquid feed direct methanol fuel cells. *J. Electrochemical Soc. 154,* 3, B352–B361.

OEDEGAARD, A. AND HENTSCHEL, C. 2006. Characterisation of a portable dmfc stack and a methanol-feeding concept. *J. Power Sources 158,* 1, 177–187.

PEI, H., HONG, L., AND LEE, J. Y. 2006. Polymer electrolyte membrane based on 2-acrylamido-2-methyl propane-sulfonic acid fabricated by embedded polymerization. *J. Power Sources 160,* 2, 949–956.

QIAN, W., WILKINSON, D. P., SHEN, J., WANG, H., AND ZHANG, J. 2006. Architecture for portable direct liquid fuel cells. *J. Power Sources 154,* 1, 202–213.

SCOTT, K., ARGYROPOULOS, P., AND SUNDMACHER, K. 1999. A model for the liquid feed direct methanol fuel cell. *J. Electroanalytical Chem. 477,* 2, 97–110.

STEELE, B. C. H. 2001. Material science and engineering: the enabling technology for the commercialisation of fuel cell systems. *J. Materials Science 36,* 5 (March), 1053–1068.

SUN, P., XUE, G., WANG, C., AND XU, J. 2009. New numerical techniques for a three-dimensional liquid-feed direct methanol fuel cell model. *SIAM J. Appl. Math. 70,* 2, 600–620.

TURONI, F., MLYNSKI, M., SADATSAKAK, A., AND SCHREIBER, M. 2005. Model based of a controller for fuel cell systems. In *Proceedings of the Model-Based Design Conference*. 116–124.

VEGA-LEAL, A. P., PALOMO, F. R., BARRAGAN, F., GARCIA, C., AND BREY, J. J. 2007. Design of control systems for portable PEM fuel cells. *J. Power Sources 169,* 1, 194–197.

WANG, Z. H. AND WANG, C. Y. 2003. Mathematical modeling of liquid-feed direct methanol fuel cells. *J. Electrochemical Soc. 150,* 4, A508–A519.

WEST, R. AND PARMER, G. 2006. A software architecture for next-generation cyber-physical systems. In *Proceedings of the NSF Workshop On Cyber-Physical Systems: Research Motivation, Techniques and Roadmap*.

WISHART, J., DONG, Z., AND SECANELL, M. 2006. Optimization of a pem fuel cell system based on empirical data and a generalized electrochemical semi-empirical model. *J. Power Sources 161,* 2, 1041–1055.

XIE, C., PAVIO, J., HALLMARK, J., BOSTAPH, J., AND FISHER, A. 2002. Key requirements of micro fuel cell system for portable electronics. In *Proceedings of the Intersociety Energy Conversion Engineering Conference*. 603–606.

XUE, D. AND DONG, Z. 1998. Optimal fuel cell system design considering functional performance and production costs. *J. Power Sources 76,* 1, 69–80.

YANG, X., ZHOU, Z., CHO, H., AND LUO, X. 2006. Study on a PZT-actuated diaphragm pump for air supply for micro fuel cells. *Sensors Actuators A: Physical 130–131*, 531–536.

ZHANG, F., SZWAYKOWSKA, K., WOLF, W., AND MOONEY, V. 2008. Task scheduling for control oriented requirements for cyber-physical systems. In *Proceedings of the Real-Time Systems Symposium*. IEEE Computer Society, Los Alamistos, CA, 47–56.

Received February 2010; revised September 2010, February 2011; accepted June 2011